Journal of Power Sources 217 (2012) 470–478

Contents lists available at SciVerse ScienceDirect

Journal of Power Sources

journal homepage: www.elsevier.com/locate/jpowsour

Determining the effective thermal conductivity of compressed PEMFC GDLs through thermal resistance modelling

J. Yablecki, A. Bazylak*

Microscale Energy Systems Transport Phenomena Laboratory, Dept. of Mechanical & Industrial Engineering, Faculty of Applied Science and Engineering, University of Toronto, 5 King's College Road, Toronto, ON, Canada M5S 3G8

HIGHLIGHTS

- Effective thermal conductivity increased with increasing compression and GDL thickness.
- Core thermal conductivities are higher than bulk values by a factor of 2.87–7.79.
- Compared to PTFE addition, high porosity surfaces dominate thermal conductivity.

ARTICLE INFO

Article history:
Received 27 March 2012
Received in revised form
1 June 2012
Accepted 3 June 2012
Available online 16 June 2012

Keywords:
Effective thermal conductivity
Gas diffusion layer
Heterogeneous porosity profile
Anisotropy
Compression
Thermal resistances

ABSTRACT

In this work, the effective through-plane thermal conductivities for compressed, anisotropic and heterogeneous polymer electrolyte membrane (PEM) fuel cell gas diffusion layers (GDLs) were determined analytically from representative physical GDL models, which were informed by microscale computed tomography imaging of four commercially available GDL materials. The number of fibre-to-fibre contact points and corresponding contact areas were extracted from these physical models as inputs to a thermal resistance model. It was found that the effective thermal conductivity increased with increasing GDL thickness (with bulk porosity remaining almost constant). The analytical model was employed to determine the bulk thermal conductivity as well as the thermal conductivity of the core region of the material. By isolating the core region from the bulk, a better understanding of the effect of the heterogeneous porosity profiles on the through-plane thermal conductivity was determined and discussed. Unlike the bulk thermal conductivity, the thermal conductivity of the core region was not dependent upon the material thickness. It was also found that the surface transition regions of the porosity distributions have a dominating effect over the addition of PTFE in impacting the overall thermal conductivity.

1. Introduction

Achieving proper heat management within a polymer electrolyte membrane (PEM) fuel cell is critical for improving its performance and lifetime. Heat produced from the electrochemical reaction and water phase change results in temperature gradients across a single cell and fuel cell stack [1–5]. Careful control of the temperature throughout the cell is important for avoiding membrane dehydration and degradation [4]. The temperature within the fuel cell affects the relative humidity, membrane water content, saturation pressure, and reaction kinetics, which are coupled together in their impact on the overall performance of the fuel cell. Due to the coupled nature of these parameters, numerical modelling is a powerful means of designing the PEMFC, and in particular, designing the microscale features of the individual components. However, accurately modelling the heat transfer rates and temperature distributions within a fuel cell requires knowledge of the thermal transport properties of individual materials, in particular, the effective thermal conductivity.

The main path for heat removal from the PEM fuel cell membrane to the current collectors is through the gas diffusion layer (GDL), otherwise known as the diffusion medium (DM) or porous transport layer (PTL), and the rate of heat removal is therefore largely dependent upon the thermal transport properties of the GDL. Although a number of analytical correlations exist for the effective thermal conductivity of a composite material with varying geometries [6], the GDL thermal conductivity can be estimated but not accurately represented by a single analytical correlation due to the anisotropic [7] and heterogeneous nature [8] of

* Corresponding author. Tel.: +1 416 946 5031; fax: +1 416 978 7753.
E-mail address: abazylak@mie.utoronto.ca (A. Bazylak).

0378-7753/$ – see front matter © 2012 Elsevier B.V. All rights reserved.
http://dx.doi.org/10.1016/j.jpowsour.2012.06.011

the fibres within the GDL. Through a compact analytical model of the GDL, Sadeghi et al. [9] calculated the through-plane effective thermal conductivity of the GDL using an idealized repeating unit cell to represent the GDL structure. The analytical model accounted for: the conduction through the solid fibrous material and gas phase, the thermal constriction resistance at the regions of fibre-to-fibre contact, and gas rarefaction in the microgaps to determine the effective thermal conductivity. The results from their model [9] and parametric study showed that the thermal constriction resistance dominates the total thermal resistance in the determination of the effective thermal conductivity.

The work of Sadeghi et al. [9] was extended by the same authors to include an experimental and analytical study on the effective thermal conductivity and thermal contact resistance of the GDL under a compressive load [10]. Increases in the bipolar plate pressure were found to increase the thermal conductivity. Further to this approach, Sadeghi et al. [11] recently reported the first combined experimental and analytical study on the in-plane effective thermal conductivity and thermal contact resistance of the GDL. Their analytical model accounted for heat conduction through randomly oriented fibres, the contact area between fibres, and polytetrafluoroethylene (PTFE) covered regions. The results from their analytical model and experimental work indicated that PTFE has little impact on the in-plane thermal conductivity. The results obtained for the in-plane thermal conductivity were 12 times higher than the through-plane thermal conductivity from their previous work.

The effective thermal conductivity of the GDL can be determined in-situ from the temperature of an operating fuel cell. Ex-situ experiments for the GDL are more common than in-situ experiments due to the challenges associated with the complexity of coupled processes within an operating fuel cell [12]. The first experimentally determined GDL thermal conductivity was reported by Vie and Kjelstrup in 2003 [13]. Khandelwal and Mench [14] measured the through-plane thermal conductivity of a dry Nafion membrane and Sigracet and Toray carbon paper GDLs in a steady-state ex-situ experiment. The results presented by the authors revealed that the thermal conductivity is a function of the GDL PTFE content. The thermal conductivity of an untreated Sigracet GDL was two times larger than the thermal conductivity of a Sigracet GDL treated with 20% PTFE. Burheim et al. [12] reported experimental measurements for the anisotropic through-plane effective thermal conductivity of dry and wet Nafion membranes and compressed GDLs from ex-situ experiments. Compression was shown to cause a nearly linear increase on the effective thermal conductivity with applied compression load. Burheim et al. [15] recently reported an extensive study on the effective through-plane thermal conductivity of a number of GDL materials. The authors [15] studied the effect of residual water, PTFE content, and compression on the through-plane thermal conductivity and the thermal contact resistance between the GDL and aluminium bipolar plate. The through-plane thermal conductivity was found to decrease with increasing PTFE content.

Sadeghi et al. [9] provided important insight into the through-plane thermal conductivity of the GDL with an analytical model considering the case of an untreated and periodically ordered GDL structure. In practice, the GDL is anisotropic and carbon paper GDL materials are composed of randomly oriented fibres. Recent work by Fishman et al. [8] indicated that the porosity of the GDL is heterogeneous. Burheim et al. [15] attributed experimentally found trends in the through-plane thermal conductivity with the GDL thickness of carbon paper materials to this heterogeneity. A numerical investigation into the impact of GDL porosity heterogeneity on effective thermal conductivity would be highly informative for designing GDL materials for optimized heat transfer properties, which would lead to overall improved fuel cell performance.

In this work, an analytical model is used to determine the effective through-plane thermal conductivity of commercially available GDL materials based on the heterogeneous porosity profiles previously published in [8,16]. The effects of the heterogeneous porosity distribution, GDL compression, and PTFE content on the effective thermal conductivity are investigated. The results of the model are compared with experimental data presented by Burheim et al. in Ref. [15].

2. Model development

Our approach to determining the effective through-plane thermal conductivity of the GDL consists of two steps: the representative physical GDL model and the thermal resistance model. Based on the findings of Sadeghi et al. [9,10] where heat transfer was found to be dominated by fibre-to-fibre contact, our analytical model will only consider heat transfer through fibre-to-fibre contact points. Using inputs of porosity, GDL compression pressure, and in the case of treated materials, PTFE distributions, the representative physical GDL model is used to determine the number of fibre-to-fibre contact points throughout the domain and the contact area dimensions of the contact points. These dimensions are then used as inputs to the thermal resistance model for determining the effective thermal conductivity of the GDL.

2.1. Fibre representation

To model the effective through-plane thermal conductivity of the GDL, a representative modelling domain, shown in Fig. 1, with width, W, and length, L, was constructed for a number of randomly oriented fibres, N_t, in the x–y plane. The fibres are immersed in quiesent air, each with a length and diameter of l and d, respectively. Layers of the fibres are stacked vertically through the entire thickness, H, of the GDL modelling domain. The geometric parameters of the modelling domain are shown in Table 1.

The through-plane porosity distributions reported in Ref. [8] of four GDL materials are employed in this work to establish the number of fibres, in each layer, t, of the modelling domain. The porosity of each layer can be found from:

$$\varepsilon_t = 1 - \frac{V_{\text{solid}}}{V_{\text{total}}} \tag{1}$$

where V_{solid} is the total volume of the solid carbon fibres, and V_{total} is the total volume of modelling domain. Based on the volume of the modelling domain used and the prescribed porosity of each layer, the number of fibres required in each layer, N_t is determined from:

$$N_t = (1 - \varepsilon_t)\frac{LWt}{\frac{\pi d^2}{4} l} \tag{2}$$

where d and l are the diameter and length of the carbon fibre, respectively.

In our model, the number of contact points, C_f, for a single fibre in layer, t, and the adjacent layer, $t+1$, is a function of the porosity of both layers (i.e. number of fibres in each layer, N_t) and the orientation angle of the fibre, θ. The fibres are oriented in the modelling domain with a uniform distribution of randomly chosen angles between 0 and 90° (in the X–Y plane). The maximum number of contact points for a given fibre in each layer occurs when the fibre orientation angle is 90°, as shown in the periodically ordered fibre arrangement (Fig. 2). The minimum number of

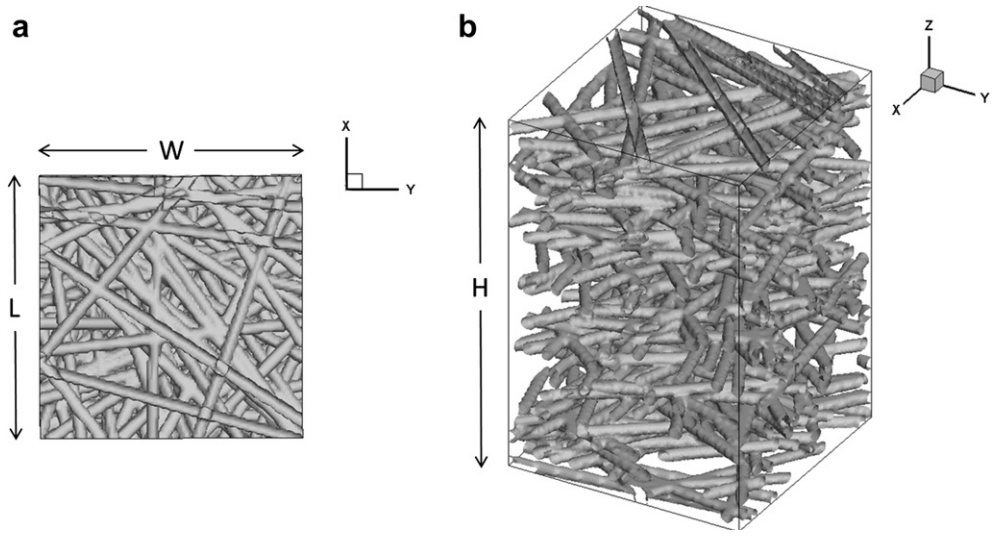

Fig. 1. Schematic illustrating a section of the representative physical model, which consists of solid, continuous fibres oriented in a planar direction a) X–Y plane orientation, and, b) isometric view.

contact points is seen when θ is 0° between the two layers. A non-linear relationship was determined for the number of contact points for a single fibre in a layer with porosity, ε_t, based on its orientation angle (Fig. 3a). The average number of contact points for a single fibre, C_f, in a layer with porosity, ε_t, was determined from this relationship and is used as an input into the model. The average number of contact points, $C_{f,avg}$, was found to vary linearly with porosity and is interpolated for each porosity value, ε_t (Fig. 3b), when generating the thermal resistance model.

2.2. Compression

In practice the PEM fuel cell is compressed during assembly. It is important to consider the effect of this compression on both the individual carbon fibres and on the overall GDL. Here, it assumed that the fibres do not bend under compression, and the only deformation of the fibres is at the contact area between two fibres. The application of a load will create a contact area between two fibres that is finite but small when compared with the dimensions of the fibres [17]. The overall thickness of the GDL will change due to compression. These considerations are described in detail in the following subsections.

2.2.1. Fibre compression

Based on the assumption that both fibres are smooth, a smooth, non-conforming contact area between the two fibres is formed, which is a function of the force applied on the fibres, F, the Young's modulus of the fibre (210 GPa), E_f, and the angle between the two fibres, θ. The material properties of the fibres are shown in Table 2.

When cylindrical fibres contact each other eccentrically, the contact region is considered elliptical [17]. The Hertzian theory of contact is used to predict the shape of contact between solids and how it grows under an increasing load [17]. Following the analytical modelling approach for the GDL presented by Sadeghi et al. [9], the application of the Hertzian contact theory for non-conforming smooth cylinders is used to define the elliptical contact region, described by the major and minor semi axis, a and b. The detailed formulation for this theory can be found in Sadeghi et al. [9] and Johnson [17].

It is assumed that fibres will not bend and new contact points will not be created under compression. However, under compression, it is assumed that the existing contact area between two fibres will increase. The contact load, F, for each contact point can be expressed in terms of the pressure within the GDL, P_{GDL}, the cross-sectional area of the unit cell defined by L and W, and the number of contact points for a given layer, C_t [9]:

$$F_{\max,t} = \frac{P_{GDL}LW}{C_t} \tag{3}$$

2.2.2. GDL compression

In this work, we employed the porosity profiles and material thicknesses for the uncompressed materials measured in our group's previous work [8]. To account for the compression of the GDL, we employed Hooke's law to determine the compressed thickness of the material. Assuming the deformation of the GDL is elastic, ξ, the strain from the GDL compression is given by:

$$\xi = P_{GDL}/E_{GDL} \tag{4}$$

where E_{GDL} is the Young's modulus of the GDL material. The compressed thickness, H_c, is determined from:

Table 1
Unit cell geometry properties employed to generate the representative physical model.

Fibre diameter, d	Fibre length, l	Unit cell width, W	Unit cell length, L
7.32 μm	325 μm	1500 μm	1625 μm

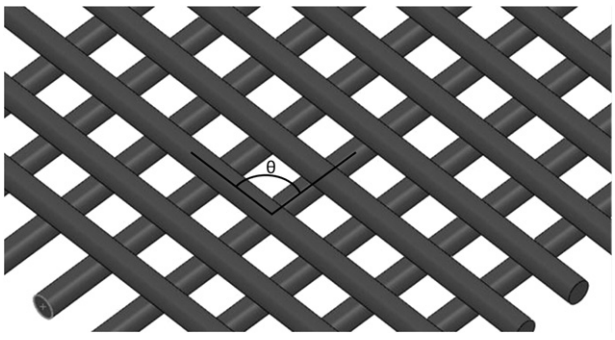

Fig. 2. Schematic illustrating a periodically ordered fibre arrangement with $\theta = 90°$.

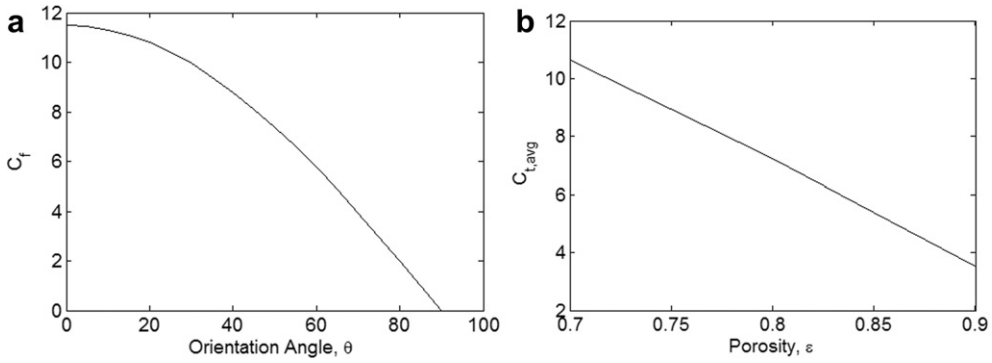

Fig. 3. (a) Contact points per fibre in layer, *t*, within the defined unit cell with a porosity of 80% as a function of the orientation angle, and, (b) average number of contact points as a function of porosity.

$$\xi = \frac{H_o - H_c}{H_o} \tag{5}$$

where H_o is the uncompressed thickness of the GDL. A value of 17.9 MPa for the Young's modulus of Toray carbon paper was used [18].

The analytical model assumes that compression is applied uniformly within the GDL. It is important to note that, this is not the case during fuel cell operation as there will be higher compression in areas under the lands of the bipolar plate than in areas under the channels [12].

2.3. PTFE treatment

For the GDL materials considered that have PTFE treatment, the method of incorporating the PTFE in our analytical model is adopted from previous modelling of the effective thermal conductivity in the in-plane direction by Sadeghi et al. [11]. The bulk porosity with the addition of PTFE, ε, is calculated with the general form of the equation:

$$\varepsilon = \varepsilon_0 - \rho\frac{\lambda(1-\varepsilon_0)}{1-\lambda} \tag{6}$$

where ε_0 is the bulk porosity of the material before PTFE is added, λ is the weight fraction of PTFE, and ρ is the density ratio between carbon fibre and PTFE [19]. A value of 0.9 is used for ρ [18].

In recent experimental work by Rofaiel et al. [20], the relative through-plane distribution of PTFE in Toray-TGP-H-090 was quantified using scanning electron microscopy (SEM) energy dispersive X-ray spectrometry (EDS) imaging. Results from this work revealed an almost symmetrical presence of PTFE in the paper GDL material with a lower accumulation in the centre region and peaks of accumulation towards the surfaces. The experimentally measured PTFE distributions from the previously published work of Rofaiel et al. [20] are employed in this investigation to inform the non-uniform distribution of PTFE.

The total weight fraction of PTFE in a GDL sample, λ, is known *a priori* from supplier specifications, and when combined with the relative through-plane distribution of PTFE provided by Rofaiel et al. [20], the heterogeneous distribution of PTFE in the through-plane direction of the GDL can be extracted. In other words, the non-uniform weight fraction of PTFE at each layer, λ_t, in the through-plane direction of the domain is determined for this investigation from supplier specifications combined with the measurements reported in Ref. [20].

To fully define the modelling domain, the number of fibres, N_t, as well as the weight fraction of PTFE, λ_t, must be prescribed at each through-plane position (layer) of the GDL. The through-plane porosity distributions reported in Refs. [8,16] were employed; however, Fishman et al. reported porosity distributions that accounted for both PTFE and carbon fibres. Therefore, in order to extract N_t, it is first necessary to determine the porosity at each through-plane position of the material in the absence of PTFE addition (fibre porosity), $\varepsilon_{0,t}$, by using Eq. (5). Once N_t is extracted, the same procedure for Fibre Representation and Fibre Compression outlined in Sections 2.1 and 2.2 for untreated GDL materials can be followed.

Table 2
Carbon fibre properties employed for representative physical model.

Thermal conductivity, k	Poisson's ratio, υ	Young's modulus, E_f
120 W/m K [7]	0.3 [9]	210 GPa [9]

2.4. Thermal model

The effective thermal conductivity is a porous media property that accounts for the contributions of the thermal conductivity of each phase present [21]. For the determination of the effective thermal conductivity of the GDL, the two phases that are generally considered are solid carbon fibres and gaseous air with values of thermal conductivity of 120 W/m K and 0.03 W/m K, respectively [22].

For the analytical model presented here, it is assumed that the only heat transfer is steady-state, one-dimensional (1-D) conduction in the through-plane direction of the GDL. With the calculation of the Grashof and Peclet numbers, Ramousse [7] showed that natural convection and convective heat transfer are negligible compared with conduction in the GDL. Radiative heat transfer can be neglected for temperatures below 1000 K [23], which is well above the operating range of a PEM fuel cell. Therefore, heat is transferred through the modelling domain from fibre-to-fibre contact only. The thermal resistance in the conduction along a fibre is ignored, as it is assumed to be negligible compared with the thermal constriction and spreading resistances [9].

A thermal resistance network or circuit can be constructed for 1-D heat transfer with no internal energy generation and with constant properties [24]. The thermal resistance, $R_{t,\mathrm{cond}}$, for conduction in a plane wall is defined by:

$$R_{t,\mathrm{cond}} = \frac{\Delta T}{q} = \frac{L}{kA} \tag{7}$$

where ΔT is the difference in temperature across the wall, q is the heat flux, L is the length of the plane wall, k is the thermal conductivity of the wall, and A is the cross sectional area of the wall. An equivalent thermal circuit with thermal resistances in parallel and series is analogous to an electrical circuit governed by Ohm's law.

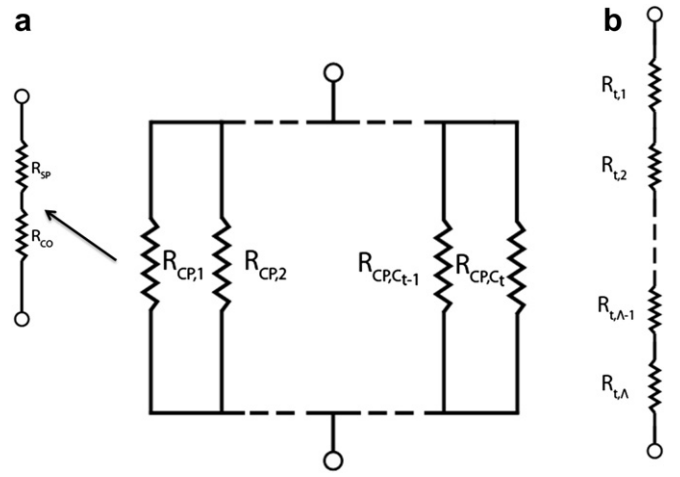

Fig. 4. (a) Equivalent thermal resistance network of a single layer with C_t number of contact points, and (b) the equivalent thermal resistance network through the GDL thickness with Λ number of layers.

The dominant thermal resistance for heat conduction through the GDL is the thermal constriction and spreading resistance [10]. The thermal spreading resistance, $R_{sp,}$ is equivalent to the thermal constriction resistance, $R_{co,}$ and accounts for the thermal energy that is transferred between the two fibres at the contact interface. When the dimensions of the contact area are very small compared with the dimensions of the contacting bodies, the heat transfer through the contact area is constrained, and the solution can be modelled as a heat source on a half-space [25]. Heat entering the half-space is constricted to flow through the small contact area (thermal constriction resistance), and heat leaving the half-space spreads out from the contact area (thermal spreading resistance [25]. In the case of the GDL, the contact area between the two fibres is considered as the heat source, and the much larger carbon fibres are considered as the half space.

The thermal constriction resistance is then a function of the elliptical contact area calculated with the Hertizan contact theory and described by the major and minor semi-axis of the elliptical contact area, a and b, respectively. Using the work of Yovanovich [26] that resulted in half-space solutions for different contact interfaces, Sadeghi et al. [9] expressed the thermal constriction resistance analytically to be:

$$R_{co} = \frac{1}{2\pi k_s a} K(\eta) \tag{8}$$

where $K(\eta)$ is the complete elliptical integral and a function of the contact area dimensions, a and b. The total thermal resistance at a fibre contact point, R_{cp}, is given by:

$$R_{CP} = \left[R_{co} + R_{sp}\right]^{-1} \tag{9}$$

The total thermal resistance for each layer, R_t (Fig. 4a), within the modelling domain can be found from the summation of each individual thermal resistance of each contact point in parallel:

$$\frac{1}{R_t} = \sum_{0}^{C_t} \frac{1}{R_{CP}} \tag{10}$$

The total resistance in the modelling domain, R_{total} (Fig. 4b), can be found as a series summation of the thermal resistances of each layer, for a total of Λ layers in the domain:

$$R_{total} = \sum_{0}^{\Lambda} R_t \tag{11}$$

The effective thermal conductivity can be found from the total thermal resistance:

$$k_{eff} = \frac{t_{total}}{R_{total} A} = \frac{H - t}{R_{total} WL} \tag{12}$$

When considering GDL materials treated with PTFE, the approach outlined above is followed, and only heat transfer through fibre-to-fibre contact is considered. The PTFE distribution within the GDL can vary with method of application, but for the purpose of this analytical model only PTFE that has accumulated at fibre contact points will be considered. An equivalent thermal resistance at each fibre-to-fibre contact point is constructed to include the addition of PTFE. The location of PTFE at a contact point and the equivalent thermal resistance diagram is given in Fig. 5. The total thermal resistance at a fibre contact point, R_{cp}, is given by:

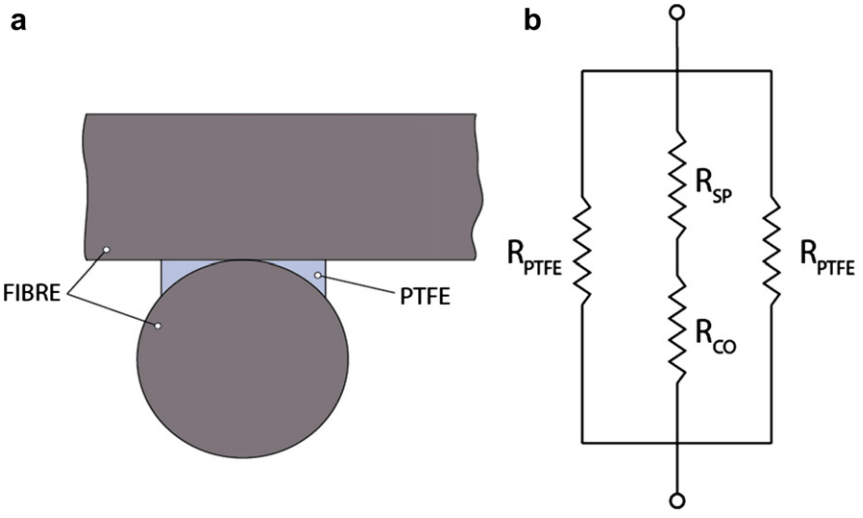

Fig. 5. (a) Schematic illustrating a single fibre-to-fibre contact point for treated carbon paper, and (b) the equivalent thermal resistance network for (a).

$$R_{cp} = \left[(R_{PTFE})^{-1}+(R_{co}+R_{SP})^{-1}+(R_{PTFE})^{-1}\right]^{-1} \quad (13)$$

The thermal resistance of the PTFE is given by:

$$R_{PTFE} = \frac{1}{\pi k_{PTFE} r}\left[\int_{\alpha}^{\beta}\frac{u\,du}{1-\sqrt{1-u^2}}\right]^{-1} \quad (14)$$

where α and β are parameters developed by Sadeghi et al. to describe PTFE [11]. The proposed relations from Sadeghi et al. [11] describe the geometry of the portion of PTFE that has accumulated at a contact point from SEM images of carbon paper GDL with varying PTFE wt. content. The thermal conductivity of PTFE is 0.649 W/m K [11]. The parameter, α, gives the radius ratio of contact area to fibre. A value of 0.1 was estimated from SEM images by Sadeghi et al. [11] and is also used in this study. The parameter β_t is the radius ratio of PTFE to carbon fibre and varies with the amount of PTFE with the following relationship in the through-plane direction [11]:

$$\beta_t = 0.25 + 3(\lambda_t - 0.05) \quad (15)$$

where λ_t is weight fraction of PTFE at each layer in the through-plane direction. As before, the total thermal resistance for each layer, R_t, within the modelling domain can be found from the summation of each individual thermal resistance of each contact point in parallel. The total resistance in the modelling domain, R_{total}, can be found as a series summation of the thermal resistances of each layer.

3. Results

The analytical model was implemented with heterogeneous through-plane porosity distributions for Toray carbon paper TGP-H-030, 060, 090, and 120 obtained through X-ray microscale computed tomography (μCT) experiments conducted in Ref. [8,16]. The GDL materials considered were uncompressed and did not have a microporous layer (MPL). The spatial resolution for the μCT data gathered is 2.44 μm [8,16]; however, for the purpose of this model, measurements for porosity are interpolated from the experimentally determined data set at every 7.32 μm through the thickness of the GDL. The details of the microscale computed tomography visualization are presented in Ref. [8,16].

3.1. Untreated paper

The effective through-plane thermal conductivity obtained from the analytical model is shown in Table 3 for three compression pressures, P_{bp}. The effective thermal conductivity results for varying compression pressures from the analytical model are also shown in Fig. 6 and compared with experimental data for Toray carbon paper GDL materials presented by Burheim et al. [15]. The results from the analytical model are in agreement within 11.6%, 7.6%, and 4.0% of the experimentally obtained results from Ref. [15] for Toray TGP-H-060, 090, 120, respectively averaged over the range of compression pressures. Similar trends can be seen between both sets of data, as described below.

The effective thermal conductivity is observed to increase with increasing compression pressure. As noted by Burheim et al. [15], and shown in Fig. 6, the effective thermal conductivity increases almost linearly with increasing compression pressure. The results from the analytical model also display another trend noted in the experimental work by Burheim et al. [15] for Toray carbon GDL material with varying thickness. As shown in Fig. 6, the effective thermal conductivity increases with increasing GDL thickness (even as the average bulk porosity remains approximately constant) for all three GDL materials presented by Burheim et al. [15]. The results presented in Fig. 6 for the analytical model follow this trend except for Toray TGP-H-060 and 090. The effective thermal conductivity of Toray TGP-H-060 is an average of 3% higher than Toray TGP-H-090. To further explore the reason for this trend, the effective thermal conductivity for each GDL material is presented as a function of through-plane position in Fig. 7.

Table 3
Effective thermal conductivity of untreated Toray paper GDLs for different compression pressures.

P_{GDL} (kPa)	H (μm)	$\varepsilon_{bulk,avg}$ (%)	k_{eff} (W/m K)
Toray TGP-H-030			
460	114.11	82.50	0.2165
930	111.03	82.01	0.3233
1390	108.02	81.51	0.4099
Toray TGP-H-060			
460	213.96	81.62	0.4505
930	208.18	81.11	0.6039
1390	202.54	80.58	0.7327
Toray TGP-H-090			
460	290.03	82.00	0.4268
930	282.2	81.50	0.5945
1390	274.55	80.98	0.7317
Toray TGP-H-120			
460	349.46	78.13	0.6111
930	340.03	77.52	0.8329
1390	330.81	76.89	0.9851

As shown in Fig. 7, the thermal conductivity through the thickness of the GDL is strongly dependent upon the local value of the porosity, ε_t. For all four GDL materials presented, the Toray carbon paper materials display local porosity minima and maxima throughout the thickness [8]. At the location of a porosity minimum, a maximum local value of thermal conductivity is observed. The four materials investigated have a local maximum value of thermal conductivity between 2.5 and 3.0 W/m K.

Fishman et al. [8] noted that the heterogeneous porosity distributions for all four GDL materials are distinct and consist of three segments: two transitional surface regions and a core region. The transitional surface region extends linearly between the outer

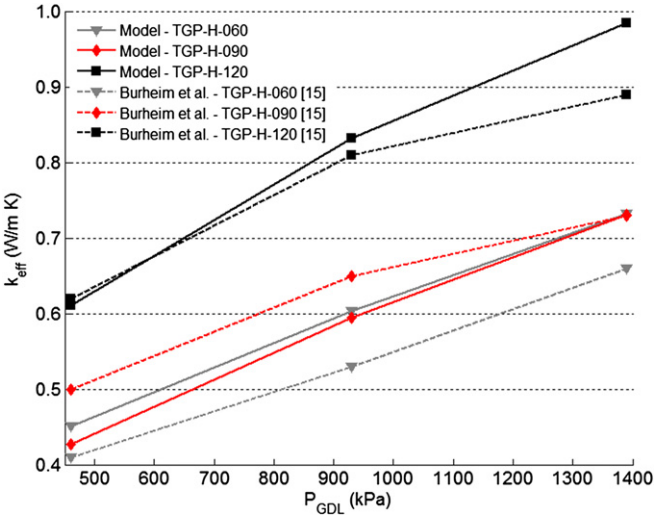

Fig. 6. Comparison of measured average effective thermal conductivity with compression pressure and with values from Burheim et al. [15].

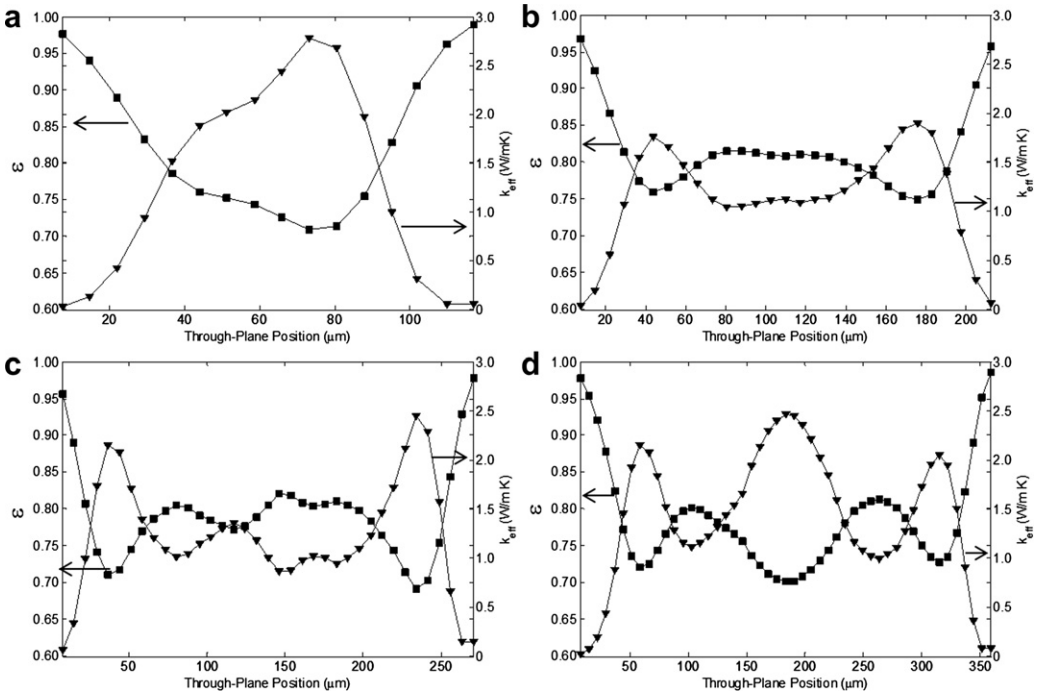

Fig. 7. Through-plane effective thermal conductivity and porosity distributions for untreated (a) Toray TGP-H-030, (b) Toray TGP-H-060, (c) Toray TGP-H-090, and (d) Toray TGP-H-120.

surfaces and the local porosity minima and the core region is between the two transitional surface regions (see Fig. 8) [8]. After isolating the core region in the analytical model, the effective thermal conductivity of this region was determined. Core region thermal conductivity results are presented in Table 4 for a single compression pressure, P_{bp}, of 460 kPa and compared with the overall bulk effective thermal conductivities. The core thermal conductivity is 7.79, 2.87, 3.74, and 3.31 times higher than the overall bulk thermal conductivity for Toray TGP-H-030, 060, 090, and 120, respectively. Unlike the overall bulk thermal conductivity, the thermal conductivity of the core region is not dependent upon the material thickness.

3.2. PTFE treated paper

The analytical model was implemented with heterogeneous through-plane porosity distributions for Toray carbon paper TGP-H-060 obtained Ref. in [8,16] for four PTFE weight contents; 0, 5, 10, and 20 wt.%. The effective through-plane thermal conductivity obtained from the analytical model is shown in Fig. 9a at a single compression pressure, P_{bp}, of 460 kPa. The results in Fig. 9a show an increase in the effective thermal conductivity initially as PTFE is added to the material (from 0 to 5 wt.%) and then decrease as the amount of PTFE increases above 5 wt.%. The results displayed in Fig. 9a are counter-intuitive, as it was expected that the thermal conductivity would increase with increasing PTFE. As PTFE is added, additional pathways in the through-plane direction are created for heat transfer. To better understand the decrease in the thermal conductivity with increasing PTFE, an alternate method of applying PTFE in the analytical model was investigated.

In this alternate method, a single through-plane porosity distribution of Toray TGP-060 with 0 wt.% PTFE was employed. The desired amount of PTFE was subsequently added to the material following the approach outlined in Section 2.4 at each layer in the modelling domain. The effective through-plane thermal conductivity obtained from the analytical model is shown in Fig. 9b for the alternate method at a single compression pressure, P_{bp}, of 460 kPa. The results in Fig. 9b show that the effective thermal conductivity

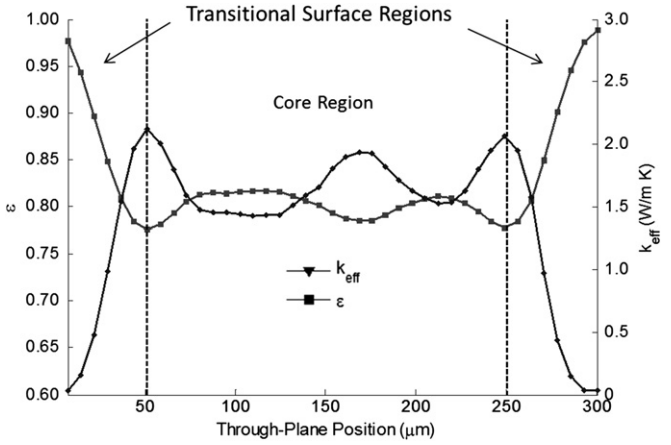

Fig. 8. Through-plane effective thermal conductivity and porosity distributions for Toray TGP-H-090 depicting core region defined by Fishman et al. [8].

Table 4
Effective thermal conductivity of untreated Toray paper GDLs: bulk and core values.

$\varepsilon_{bulk,avg}$	ε_{core}	$k_{eff,\ bulk}$ (W/m K)	$k_{eff,\ core}$ (W/m K)
Toray TGP-H-030			
0.825	0.742	0.2165	1.686
Toray TGP-H-060			
0.816	0.794	0.4505	1.294
Toray TGP-H-090			
0.820	0.801	0.4268	1.596
Toray TGP-H-120			
0.781	0.760	0.4519	1.496

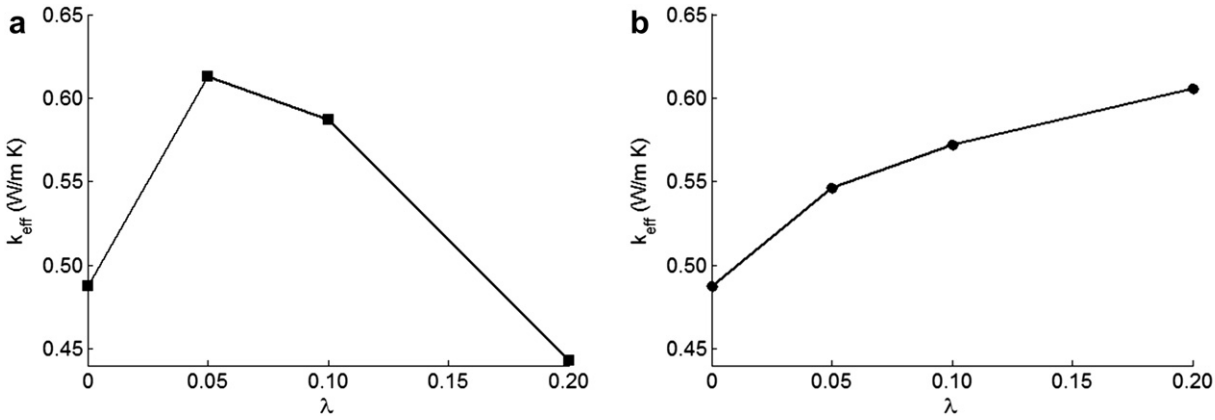

Fig. 9. Through-plane effective thermal conductivity with 0, 5, 10, and, 20 wt.% PTFE using (a) four distinct porosity profiles presented in Fishman [16] for Toray TGP-H-060 and (b) a single porosity profile of Toray TGP-H-060 with 0 wt.% PTFE employed to generate representative physical GDL models of treated GDL materials.

increases with increasing PTFE content. An increase of 24.2% with the addition of 20 wt.% PTFE is observed. These results will be discussed later in Section 4.2.

4. Discussion

4.1. Untreated paper

The effective thermal conductivity is observed to increase with increasing compression pressure (Fig. 6). This result has been previously shown in experimental [10,12,15] and analytical work [9,10] and can be explained with the analytical model presented. As the compression pressure increases, the elliptical contact area between two fibres increases. Increases in the contact area cause a decrease in the thermal constriction and spreading resistance, and subsequently, an increase in the overall thermal conductivity. Compression will also cause a decrease in the overall thickness of the GDL material that has been accounted for in this analytical model. It is important to note that while a value of 17.9 MPa was employed in this work for the Young's modulus of the GDL, within the literature, there is a large variation [18,27]; however, the model was not found to be significantly sensitive to the compressed thickness, and the trends reported in this work were not affected by the value used.

Fishman et al. [8] noted that the heterogeneous porosity distributions for all four GDL materials are distinct but each display three distinct segments: two transitional surface regions and a core region. For the thinnest GDL investigated, Toray TGP-H-030, this transitional surface region accounts for approximately 66% of its total thickness [8]. Fishman et al. [8] observed that the transitional surface region accounts for 45%, 33%, and 28% of the material thickness for Toray TGP-H-060, 090, and 120, respectively. The variation of the overall effective thermal conductivity with GDL thickness observed in Table 3 can be attributed to the relative amount of transitional surface region. The thermal conductivity appears to be strongly affected by the higher porosity values in the transitional surface regions, regardless of the overall bulk porosity value or the local maximum thermal conductivity value. This can be further explained by the results in Table 4 that compare the overall bulk thermal conductivity ($k_{eff,bulk}$) with the thermal conductivity of the core region ($k_{eff,core}$). The thermal conductivity of the core region is not dependent upon the material thickness but appears to depend on the porosity of the material.

The discrepancy between our analytical results and the experimental results from literature in Fig. 6 stems from the small variability in our experimentally obtained porosity profiles of commercially available materials. Batch-specific variations associated with the manufacturing process have been observed in these commercially available materials [28]. In this work, one sample of each GDL was employed as an input in our analytical model. Here, we see that the results in Fig. 7 from the analytical model are quite sensitive to the porosity values in the transitional regions, or locations of porosity maximums.

4.2. PTFE treated paper

The addition of PTFE in the GDL was expected to increase the effective through-plane thermal conductivity for a single compression value. Even though the thermal conductivity of PTFE is significantly lower than that of carbon fibre, the PTFE is expected to provide an additional pathway for heat transfer at a fibre contact point in the analytical model. The results from the analytical model for Toray TGP-H-060 (see Fig. 9a) show an initial increase in the thermal conductivity with the addition of 5 wt.% PTFE, followed by a counter-intuitive decrease with increasing PTFE content (from 5 to 20 wt.%).

An alternate method of PTFE application in the analytical model was used to further understand this trend. This method uses a single heterogeneous porosity distribution (0 wt.% PTFE) upon which PTFE is added, and the results for the thermal conductivity (Fig. 9b) show an increase in the thermal conductivity with increasing PTFE content (0–20 wt.%). It was observed for the untreated paper GDL materials (Fig. 6) that the thermal conductivity was strongly affected by the heterogeneous porosity distributions and the higher porosity values in the transitional surface regions, regardless of the overall bulk porosity value or the local maximum thermal conductivity value. The porosity profiles of Toray TGP-H-060 with 0, 5, 10, and 20 wt.% PTFE presented by Fishman et al. [16] are shown in Fig. 10. The addition of PTFE affects the overall shape of the through-plane porosity distribution of the material, the slope of the transitional surface regions, and the values of the porosity maxima and minima. The slopes of the transitional surface regions increases with increasing PTFE wt. content (Fig. 10). It is expected that the larger gradients in the porosity distribution at the transitional surface regions, with their associated high porosities and high thermal resistances, strongly impact the overall thermal conductivity of the PTFE treated GDL. From the results of the alternate method of PTFE application, it is observed that the surface transition regions of the porosity distributions dominate over the addition of PTFE in their impact on the overall thermal conductivity. The decrease in thermal conductivity with increasing PTFE content (from 5 to 20 wt.%) in Fig. 9(a) is therefore attributed to the dominating thermal resistances of the surface transition regions of the GDL.

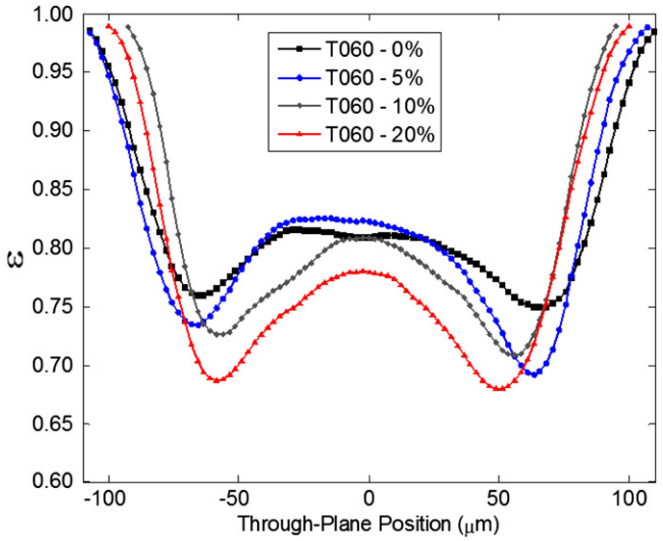

Fig. 10. Through-plane porosity distributions Toray TGP-H-060 from Fishman et al. [16] employed to generate representative physical GDL models.

5. Conclusion

An analytical model to determine the effective thermal conductivity of the GDL is presented. Representative physical GDL models informed by microscale computed tomography imaging of four commercially available uncompressed GDL materials [8,16] were employed to define the thermal model. The effect of the heterogeneous porosity distribution, GDL compression, and PTFE content on the effective thermal conductivity was investigated. The model predictions for untreated Toray carbon paper GDL materials were compared with recent experimental work by Burheim et al. [15] where two district trends were noted between both sets of data. The first trend noted was an almost linear increase in the effective thermal conductivity with increasing bipolar plate compaction pressure. The effective thermal conductivity was also seen to increase with increasing GDL thickness as bulk porosity remained almost constant. This trend was attributed to the heterogeneous porosity profiles of the material as the thermal conductivity appears to be strongly affected by the higher porosity values in the transitional surface regions, regardless of the overall bulk porosity value or the local maximum thermal conductivity value. The analytical modelling approach allows this trend to be investigated further by isolating the core region and studying its effective thermal conductivity. The effective thermal conductivity of the core region was found to be independent of the material thickness.

Two methods of applying PTFE in the analytical model were investigated to isolate the impact of the PTFE addition and the through-plane porosity distribution on the effective thermal conductivity. An initial increase in the thermal conductivity with the addition of 5 wt.% PTFE, followed by a decrease with increasing PTFE content (from 5 to 20 wt.%) was noted when four heterogeneous porosity distributions were employed in the analytical model. However, an overall increase of 24.2% in the effective thermal conductivity was noted with the addition of 20 wt.% PTFE when alternate method of PTFE application was employed, thus indicating that the overall thermal conductivity has a strong dependence on the heterogeneous porosity distributions of the treated GDL materials (in particular, the surface transition regions). The outcomes of this work provide insight into dominating effect of heterogeneity and anisotropy of the GDL on the thermal management required for improved PEMFC performance.

Acknowledgements

Funding from the Natural Sciences and Engineering Research Council of Canada (NSERC) and the Canada Foundation for Innovation (CFI) are gratefully acknowledged. Graduate scholarships received by J. Yablecki from Ontario Graduate Scholarship, NSERC, and the University of Toronto are also gratefully acknowledged.

References

[1] N. Djilali, D. Lu, Int. J. Thermal Sci. 41 (2002) 29–40.
[2] T. Berning, D.M. Lu, N. Djilali, J. Power Sources 106 (2002) 284–294.
[3] J. Ramousse, O. Lottin, S. Didierjean, D. Maillet, J. Power Sources 192 (2009) 435–441.
[4] J.G. Pharoah, O.S. Burheim, J. Power Sources 195 (2010) 5235–5245.
[5] T. Berning, N. Djilali, J. Electrochem. Soc. 150 (2003) A1589–A1598.
[6] M. Kaviany, Principles of Heat Transfer in Porous Media, Springer-Verlag, New York, 1995.
[7] J. Ramousse, S. Didierjean, O. Lottin, D. Maillet, Int. J. Thermal Sci. 47 (2008) 1–6.
[8] Z. Fishman, J. Hinebaugh, A. Bazylak, J. Electrochem. Soc. 157 (2010) B1643–B1650.
[9] E. Sadeghi, M. Bahrami, N. Djilali, J. Power Sources 179 (2008) 200–208.
[10] E. Sadeghi, N. Djilali, M. Bahrami, J. Power Sources 196 (2011) 246–254.
[11] E. Sadeghi, N. Djilali, M. Bahrami, J. Power Sources 196 (2011) 3565–3571.
[12] O. Burheim, P.J.S. Vie, J.G. Pharoah, S. Kjelstrup, J. Power Sources 195 (2010) 249–256.
[13] P.J.S. Vie, S. Kjelstrup, Electrochim. Acta 49 (2004) 1069–1077.
[14] M. Khandelwal, M.M. Mench, J. Power Sources 161 (2006) 1106–1115.
[15] O.S. Burheim, J.G. Pharoah, H. Lampert, P.J.S. Vie, S. Kjelstrup, J. Fuel Cell Sci. Technol. 8 (2011) 021013.
[16] Z. Fishman, A. Bazylak, J. Electrochem. Soc. 158 (2011) B841–B845.
[17] K.L. Johnson, Contact Mechanics, Cambridge University Press, New York, 1989.
[18] M. Mathias, J. Roth, J. Fleming, W.L. Lehnert, in: W. Vielstich, A. Lamm, H.A. Gasteiger (Eds.), Handbook of Fuel Cells: Fundamentals, Technology, and Applications, Wiley, Chichester, England; Hoboken, N.J, 2003, pp. 1–21.
[19] L. Hao, P. Cheng, J. Power Sources 186 (2009) 104–114.
[20] A. Rofaiel, J.S. Ellis, P.R. Challa, A. Bazylak, J. Power Sources 201 (2012) 219–225.
[21] J.G. Pharoah, K. Karan, W. Sun, J. Power Sources 161 (2006) 214–224.
[22] N. Zamel, X. Li, J. Shen, J. Becker, A. Wiegmann, Chem. Eng. Sci. 65 (2010) 3994–4006. 20100701.
[23] Y. Shi, J. Xiao, S. Quan, M. Pan, R. Yuan, J. Power Sources 185 (2008) 241–247.
[24] F.P. Incropera, Fundamentals of Heat and Mass Transfer, Wiley, New York, 1990.
[25] M. M. Yovanovich. “Thermal constriction resistance between contacting metallic paraboloids: application to instrument bearings.” Proc. 5th AIAA Thermophysics Conf., 1971.
[26] M.M. Yovanovich, E.E. Marotta, Heat Transfer Handbook (2003). pp. 261–393.
[27] S.G. Kandlikar, Z. Lu, T.Y. Lin, D. Cooke, M. Daino, J. Power Sources 194 (2009) 328–337.
[28] J.D. Fairweather, P. Cheung, D.T. Schwartz, J. Power Sources 195 (2010) 787–793.